Dynamic mapping of the human visual cortex by high-speed magnetic resonance imaging

(echo-planar imaging/gradient-echo/deoxyhemoglobin/magnetic susceptibility)

ANDREW M. BLAMIRE[a], SEIJI OGAWA[b], KAMIL UGURBIL[c], DOUGLAS ROTHMAN[d], GREGORY MCCARTHY[e], JUTTA M. ELLERMANN[c], FAHMEED HYDER[f], ZACHARY RATTNER[g], AND ROBERT G. SHULMAN[a]

Departments of [a]Molecular Biophysics and Biochemistry, [d]Internal Medicine, [e]Neurosurgery, [f]Chemistry, and [g]Diagnostic Radiology, Yale University, 333 Cedar Street, New Haven, CT 06510; [b]Biological Computation Research Department, AT&T Bell Laboratories, 600 Mountain Avenue, Murray Hill, NJ 07974; and [c]Center for Magnetic Resonance Research, University of Minnesota Medical School, 385 East River Road, Minneapolis, MN 55455

ABSTRACT   We report the use of high-speed magnetic resonance imaging to follow the changes in image intensity in the human visual cortex during stimulation by a flashing checkerboard stimulus. Measurements were made in a 2.1-T, 1-m-diameter magnet, part of a Bruker Biospec spectrometer that we had programmed to do echo-planar imaging. A 15-cm-diameter surface coil was used to transmit and receive signals. Images were acquired during periods of stimulation from 2 s to 180 s. Images were acquired in 65.5 ms in a 10-mm slice with in-plane voxel size of 6 × 3 mm. Repetition time (T_R) was generally 2 s, although for the long flashing periods, T_R = 8 s was used. Voxels were located onto an inversion recovery image taken with 2 × 2 mm in-plane resolution. Image intensity increased after onset of the stimulus. The mean change in signal relative to the prestimulation level $(\Delta S/S)$ was 9.7% (SD = 2.8%, n = 20) with an echo time of 70 ms. Irrespective of the period of stimulation, the increase in magnetic resonance signal intensity was delayed relative to the stimulus. The mean delay measured from the start of stimulation for each protocol was as follows: 2-s stimulation, delay = 3.5 s (SD = 0.5 s, n = 10) (the delay exceeds stimulus duration); 20- to 24-s stimulation, delay = 5 s (SD = 2 s, n = 20).

Functional mapping of the brain by nuclear magnetic resonance (NMR) methods has recently been demonstrated by two techniques. The first method uses a bolus of paramagnetic contrast agent (gadolinium/diethylenetriaminepentaacetic acid) as a tracer for blood volume (1). The agent is injected into the arm and produces variations in local blood volume magnetic susceptibility as the bolus passes through the capillary bed of the brain. The changes in susceptibility are monitored by using a transverse relaxation time (T_2)-weighted, fast magnetic resonance-imaging sequence, such as echo-planar imaging (EPI) (2) or fast low-angle shot (FLASH) (3). This method is subject to the same assumptions as all kinetic tracer methods (4), but within these restrictions it gives a quantitative result. With this method Belliveau et al. (5) have made measurements in the human visual cortex and demonstrated an increase in blood volume during stimulation. The main drawback of the technique is the need for at least two injections of contrast agent to measure the resting and activated brain states.

The second method relies solely on the paramagnetic effects of hemoglobin. In the oxygenated state (HbO_2), the molecule is diamagnetic, but once dissociated from oxygen (deoxyhemoglobin; Hb), it becomes paramagnetic. Thus, changes in Hb concentration will also result in magnetic susceptibility changes in the capillaries. Complications may arise because the paramagnetic agent is not evenly distrib-

uted throughout the blood but is compartmentalized inside the erythrocytes. Ogawa et al. (6) have studied the effect of inhaled O_2 content on the intensity of gradient-echo images of rat brain at 7 T. They have shown that a decrease in oxygen content produces dark streaks in the image corresponding to blood vessels. The increase in concentration of paramagnetic ions within the tissue decreases the apparent transverse relaxation time (T_2^*) and, hence, the signal contribution in these regions. In a subsequent paper they have also demonstrated that the contrast mechanism is blood-flow dependent by using animal models under different levels of anesthesia (7). Turner et al. (8) have used an animal model with varied levels of anoxia and shown that fast-imaging sequences can be used to follow dynamic changes in Hb. In a separate study on humans with a fast T_2^*-weighted imaging sequence at 4 T, Ogawa et al. (9) have shown that during visual stimulation there is an increase in signal intensity in the gray matter of the visual cortex relative to the unstimulated state, whereas signal from other brain regions remains unchanged. A similar increase has recently been measured by Kwong et al. (10) at 1.5 T in the visual cortex. An analogous use of the Hb method has enabled Bandettini et al. (11) to follow the effects of finger motion in the motor cortex. This Hb-based method may be difficult to quantitate because there is no control of the paramagnetic ion concentration, but it has the significant advantage that the measurements can be repeated as often as desired because no contrast medium is administered, thereby yielding improved time resolution.

We report here the results of a study using the Hb contrast method. We have used the ultra-fast EPI sequence to measure the time course of the signal changes in the human visual cortex as a function of the stimulation period.

METHODS

We studied seven normal subjects undergoing visual stimulation, as described below. (One subject was restudied on a separate occasion; the total number of studies was therefore eight.) We used the EPI technique (2) that we have implemented on our 2.1-T Bruker Biospec (Bruker, Billerica, MA) whole-body spectrometer (12), which is equipped with active shielded gradient coils (13) (Oxford Magnet Technology, Oxford, England). All subjects gave written consent for the procedure, as approved by the Human Investigation Committee of Yale University School of Medicine.

Subjects were positioned supine in the magnet. The subject's head was placed with the occipital poles at the center of a 15-cm-diameter circular surface coil and was held still by padded clamps on both sides of the head and by a third clamp

Abbreviations: EPI, echo-planar imaging; T_2, transverse relaxation time; T_2^*, apparent transverse relaxation time; Hb, deoxyhemoglobin; T_R, repetition time; TE, echo time; T_{IR}, inversion time.

on top. The back of the head was then positioned 3 cm below the isocenter of the magnet. Inversion recovery gradient-echo images [repetition time (T_R) = 2.1 s, echo time (TE) = 17.4 ms, inversion time (T_{IR}) = 810.0 ms] were acquired over four contiguous sagittal planes about the midline. From these images the calcarine fissure was located. Inversion recovery gradient-echo images (same parameters as above) were acquired, either in the axial plane or angled obliquely to maximize the inclusion of the calcarine fissure in the image. A 5-cm-diameter sphere centered at the magnet isocenter was shimmed by using all the first- and second-order shim coils and a noniterative autoshim program (14) that has been implemented on our spectrometer. In the first subject, a series of single-slice, axial, gradient-echo images were acquired with constant T_R (120 ms) and incremented TE (21–101 ms in steps of 10 ms). From these data the postshimming T_2^* in resting brain was calculated. Based on the gray-matter value (T_2^* = 70 ms), an echo time of 70 ms was chosen for the stimulation study to maximize the signal change. Acquisition of the high-resolution images and the shimming process lasted ≈1.5 hr. The spin-echo version of the EPI sequence was used for the functional imaging (see Fig. 1). The spin echo time was 28 ms, and a delay of 70 ms was introduced between the spin echo and the center of the acquisition [corresponding to the center of k-space (15)] to provide 70 ms of T_2^* dephasing. The signal from lipid in the scalp was suppressed by a frequency-selective sinc-modulated radio-frequency pulse at the lipid resonance (−305 Hz at 2.1 T) before slice selection. The EPI acquisition time was 65.54 ms (1.02 ms per echo) giving a frequency per point of 15.6 Hz in the image. The pulsed gradient (y) was doubled relative to the switched gradient (x) to improve resolution and to make full use of the reduced field of view of the surface coil. The matrix size was 64 × 64 with nominal resolution of 6 × 3 mm and a slice thickness of 10 mm. The echo-planar images were acquired with two-times oversampling (but with no increase in receiver bandwidth) to overcome nonlinearity of the k-space sampling. One half of the points per echo that most closely matched the linear k-space sample pattern was extracted and used for image construction. The shimming was optimized by hand in the imaging slice, and the linewidth of the signal from the entire selected slice was measured to be
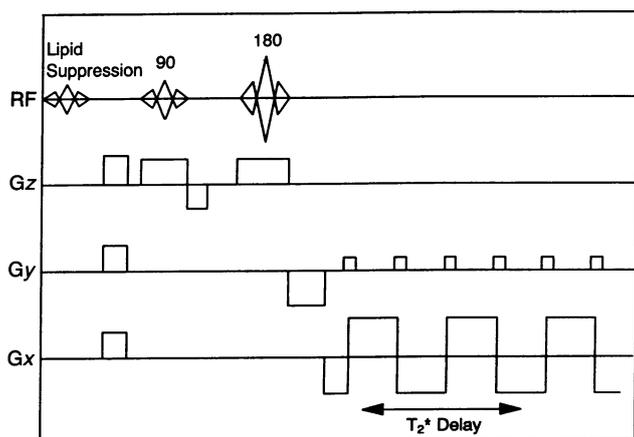
FIG. 1. Timing diagram for the spin-echo, EPI sequence. The initial stage is suppression of lipid signal from the scalp. RF, radio-frequency pulses. Slice selection is done by 90° and 180° pulses applied in a z-field gradient. The switched gradient (Gx) acts as a readout gradient, and the pulsed gradient (Gy) provides the phase-encoding. The spin-echo time (TE) was 28 ms, and the center of the EPI acquisition was offset by 70 ms ("T_2^* delay"). Matrix size was 64 × 64 (64 gradient echoes with 64 sample points per echo). Oblique planes are imaged by applying combined y and z gradients during slice selection and also by pulsing the gradients on both of these axes.

<12 Hz (which is less than the frequency per point in the image and, therefore, gives distortion-free images). In several subjects three axial, multisliced planes were acquired to encompass the entire calcarine fissure and occipital poles.

Stimulation was provided by a flashing checkerboard pattern in the eyepieces of goggles worn by the subject throughout the study (model S10SV, Grass). The stimulus rate was set at 8 Hz, which is known from positron emission tomography (PET) studies to give close-to-maximal response (16). Each stimulation period was surrounded by baseline periods of total darkness. The protocol for each study was selected from Table 1. The stimulator was controlled manually and was turned on immediately after the final prestimulus image; it was then turned off immediately after the last image of the stimulation set. The first image during stimulation therefore was at a time of one T_R into the stimulus, and the first poststimulus image was at one T_R after stimulation.

In all protocols four dummy (nonstored) scans were acquired before imaging to achieve a steady-state magnetization. In three subjects a series of pure spin-echo echo-planar images (TE = 78 ms) was acquired for comparison of the intensity changes with those in the gradient-echo images (protocols B and C). In a further two subjects, pulse rate was monitored by using a pulse oximeter deriving its signal from the subject's left toe. For each of these subjects, three dummy experiments were done (protocol C), and changes in heart rate were noted. No images were stored while the oximeter was attached because of noise injection via the oximeter cable.

Data processing was done off-line on a VAXstation 3200 computer (Digital Equipment) equipped with a SkyWarrior array processor (Sky Computers, Lowell, MA) by using home-written software. The mean control image (no stimulation) was subtracted from each image within that protocol to produce the functional images.

RESULTS

The time courses of the signal changes from a typical single pixel within the gray matter of the calcarine fissure and from a randomly selected pixel in white matter are shown in Fig. 2. In this subject, protocol B was used. The periods of activation are shown with the data. Also shown is a typical sample of the image noise from a region outside of the brain. Single-pixel results are presented to show sensitivity of the technique.

The activated region as a whole was assessed as follows. For each pixel, the mean and SD of the signal intensity were calculated for the control images (column 1 of the stimulus in Table 1). The mean value was then subtracted from the image

Table 1.   Protocols used for visual-stimulation studies

Protocol	T_R, s	Stimulus
A	2	12 OFF 10 ON 10 OFF
B	2	16 OFF 12 ON 12 OFF 12 ON 12 OFF
C	2	10 OFF 12 ON 10 OFF
D	2	10 OFF 10 ON 18 OFF 10 ON 16 OFF
E	2	10 OFF 1 ON 18 OFF 1 ON 18 OFF 1 ON 15 OFF
F	7.1	7 OFF 15 ON 10 OFF
G	4.1	10 OFF 45 ON 9 OFF

Each subject performed one or more of these tasks. The stimulus is listed in terms of number of images acquired in darkness (OFF) or with flashing checkerboard (ON). T_R is time between each image; therefore, protocol A, for example, lasted for 64 s. The stimulus was controlled by hand and was turned on immediately after the last control image (column 1 of stimulus). The first of the activated images is therefore into the stimulation by T_R s. The stimulus was turned off immediately after the final image of the stimulation period.

Neurobiology: Blamire *et al.*

Proc. Natl. Acad. Sci. USA 89 (1992)   11071
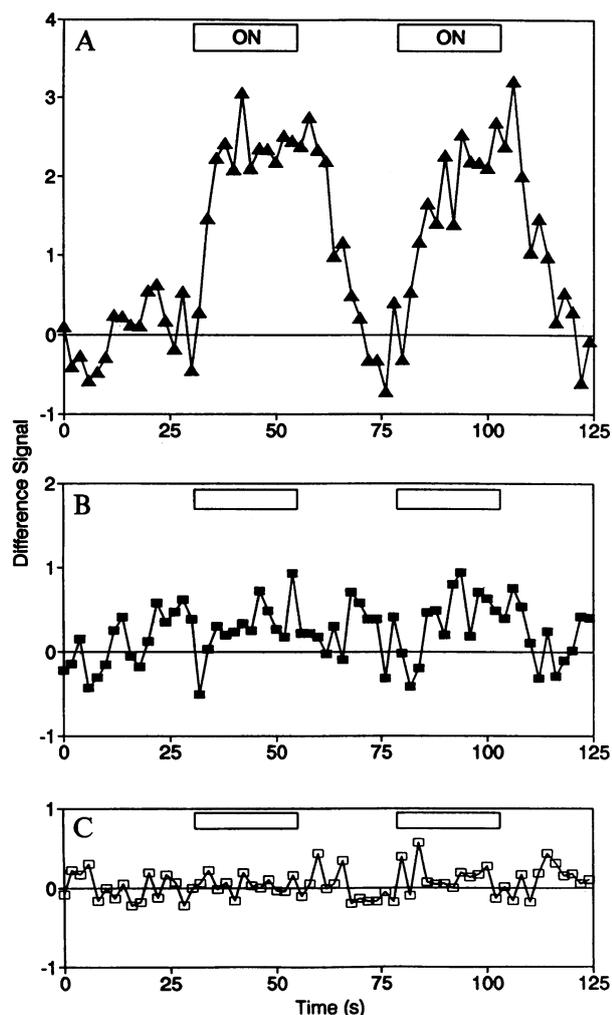
Fig. 2. Changes in image pixel intensity during visual stimulation. The three curves show single-pixel responses from gray matter in the calcarine fissure (*A*), a pixel in white matter selected randomly (*B*), and a pixel positioned outside of the head (image noise) (*C*). Images were acquired every 2 s. Protocol B was used in this study (subject 3, Table 1, $\Delta S/S$ = 0.12); periods of stimulation are shown. To produce the curves, the mean of pixel intensity in the prestimulation control images was subtracted from each image.

pixel, and the result was divided by the SD to calculate the z score for each pixel as a function of time. From the z scores, a single image was constructed showing all the pixels that changed in intensity at any point in the protocol by >3 SDs from the mean ($\approx$99% confidence limit). The time course of each of these pixels in the functional images was examined, and the total response from all activated pixels was calculated [$\Delta S(t)$]. The total mean signal intensity in the control state (*S*) for the same region of interest was also calculated.

Protocols A, B, C, and D contained stimulation periods of 20 or 24 s, which all produced similar increases in signal. Analysis of these data sets shows several clear features. Firstly, the pixel intensity in all subjects shows a time lag between start of the stimulation and increase in signal intensity. Length of the delay was measured as the time between start of the stimulation and first increase of signal intensity >3 SDs from the prestimulation mean. This value was calculated for each stimulation period in protocols A–D. The mean value of these measurements was 5 s (SD = 2 s, *n* = 20). A similar delay also occurred between end of stimulation and return to baseline signal levels (mean delay = 11 s, SD = 3 s, *n* = 20). In protocol B the delay between the two periods of activation (24 s) was found to be only just long enough to

reestablish the baseline signal, so a revised two-stimulus protocol was devised (protocol D). The accuracy of the measurement of delay is limited by the T_R of the experiment, which gives a minimum accuracy of 1 s, and also by the noise level in the subtracted data, which may mask the initial changes in intensity.

The mean change in signal (ΔS) relative to the unsubtracted signal (*S*) for the activated region was 0.10 (SD = 0.03, *n* = 20), where ΔS was measured as the maximum increase during each stimulation period. The mean value of signal change to noise was 22.5 (SD = 10.4, *n* = 20), where the noise was measured as the total magnitude in an equal number of randomly distributed pixels outside of the head. Individual subject values are shown in Table 2. The use of the z-statistic image to define the activated region of interest tends to lead to an average value for ($\Delta S/S$), which is reduced by partial volume effects. The pixel size in our experiment is large enough to encompass regions of gray and white matter in various ratios, depending on the position of the cortex relative to the imaging matrix. Regions of brain that do not exhibit activation behavior may then be added into the total response, increasing *S* but not ΔS. Individual pixels show much greater values of ($\Delta S/S$) with a maximum in one subject of 45%.

Protocols F and G contained stimulation periods of 107 and 185 s and were designed to see whether there was any accommodation by the brain to prolonged stimulation periods. Such an effect would have consequences in other modalities, such as positron emission tomography, where total data acquisition time is many seconds, and it must be assumed for quantitation purposes that the activation was constant throughout the measurement. Two protocols were used, depending on the available space for image storage at acquisition time. Again a rise in signal intensity occurred upon stimulation. Within the accuracy of our experiments the activated signal intensity was constant during the stimulation period. In these protocols the T_R was too long to permit any accurate measurement of the delay between the start of simulation and the response.

Each subject studied with 2-s periods of stimulation (*n* = 2, protocol E) was also studied with a longer period (protocols A–D). By using the same pixels seen to be activated during extended stimulation, the summed response was cal-

Table 2. Individual values of signal change and time delay

Subject	Protocol	Delay to response, s	$\Delta S/S$	$\Delta S/N$
1	A	6.0	0.12	19.9
2	B	7.0	0.10	33.4
3	B	6.0	0.12	16.4
4	B	6.0	0.07	22.0
5:1	D	4.0	0.06	6.0
	E	3.5	0.04	6.6
	G		0.06	7.9
5:2	C	4.6	0.08	14.0
6	C	4.5	0.10	27.2
	E	3.5	0.06	8.8
	F		0.05	12.7
7	C	2.0	0.12	24.3

The mean delay to activation is the mean for all pixels that show a significant change above control level (3 SDs). The delay is measured from beginning of stimulation to first significant signal increase. No delay is reported for protocols F and G because the T_R for these experiments was comparable to the delay time, giving poor accuracy in such measurements. ΔS is maximum change in signal intensity during stimulation summed over all activated pixels; *S* is summed prestimulation signal intensity for the same pixels as ΔS; *N* is summed noise measured in an equal number of pixels to *S* and ΔS. The pixels for calculating *N* were selected randomly throughout the image space outside the brain.
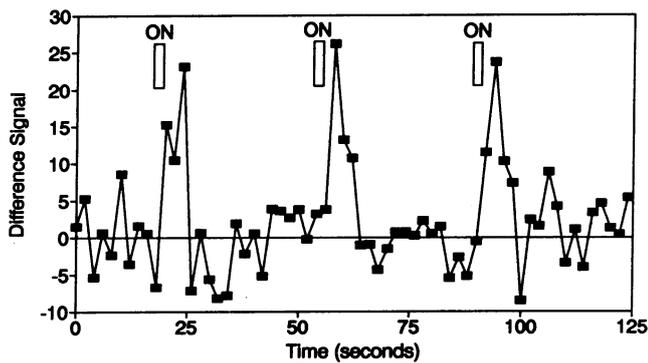
FIG. 3. Changes in image pixel intensity during 2-s periods of stimulation (protocol E, subject 5:1, $\Delta S/S$ = 0.04). The response is the total response (10 pixels) from all activated pixels. The activated region was defined by using the images acquired with protocol D on the same subject.

culated for protocol E to increase the signal-to-noise ratio. The total response for one subject is shown in Fig. 3. These results also exhibit a delay between start of the stimulus and effect. In this protocol the mean value of the delay (averaged over all stimuli and subjects) was 3.5 s (SD = 0.5 s, n = 10). Because the stimulus was only present for a 2-s period, the magnetic resonance-visible response does not overlap with the stimulus period.

The spin-echo series (protocols B and C) were analyzed in the same way as above with the accompanying gradient-echo images used as a guide to define the activated region of interest. These data sets did not show any change in image intensity above control levels during the stimulus.

The apparently random signal variation on top of the activation data is several times larger than the image noise. It is clear from Fig. 2 that the fluctuations are therefore not receiver noise. Fig. 4 shows the response taken from a single pixel at the edge of the brain, distant from the visual cortex, and clearly shows a periodic fluctuation. This response is a
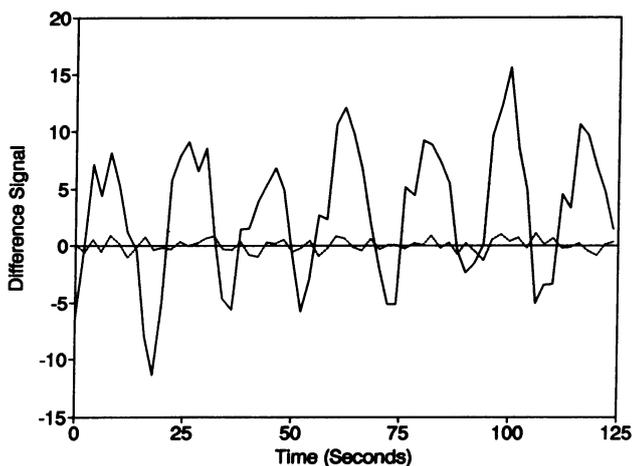
FIG. 4. Changes in image pixel intensity from mean prestimulation control image. The response is taken from a single pixel at the brain surface. The period of oscillation is ≈20 s. Pulsatile motion of the brain occurs during the cardiac cycle, producing images that expand and contract during the cycle. In this subject the mean control image (prestimulation) covers a complete cycle of the oscillation. The width of the brain in individual images oscillates about the mean; thus subtraction of the mean produces an increasing and decreasing signal. The period of the oscillation is much less than the subject's heart rate because the oscillation is highly undersampled at a 0.5-Hz rate. Also shown is a sample of the image noise for comparison. This type of response was never found in the region of the visual cortex and was not present in all subjects.

subtraction artifact caused by brain pulsation. The average control image in this case consisted of images from one complete cycle of the oscillation. Individual images in the set are, therefore, wider or narrower than the average, depending on the phase of the cardiac cycle when each was acquired. Subtraction of the average gives increased or decreased signal. Such pixel responses were not seen in all subjects and, if present, were not evident in the region of the primary visual response. These responses can be eliminated by triggering the acquisition to the subject's electrocardiograph. The inter-image delay must also then be increased to allow full relaxation of the slice between images and prevent subtraction errors due to slight variation in saturation as the heart rate changes. A similar result has recently been published where the same effect was used as a remote method for measuring heart rate (17). The experiments measuring subject heart rate showed that, although there were changes in the rate by up to 5 beats per min during the full protocol, direction of the change was not correlated to the conditions.

DISCUSSION

These results and the results of others (9, 10) show that local changes occur in image intensity in the visual cortex of normal human brain during visual stimulation that can be used for functional imaging. In addition to the spatial resolution, our results show a time lag between start of stimulation and onset of the magnetic resonance-visible changes.

The gradient-echo magnetic resonance image is sensitive not only to the intrinsic relaxation properties of the brain but also to the inhomogeneities of the static magnetic field within the sample. These inhomogeneities determine the T_2^* of the sample. This value can be subdivided into several components: the actual T_2 of the sample plus a macroscopic term due to imperfect shimming of the main field and a microscopic term due to compartmentalized paramagnetic ions within the capillaries. We have minimized the macroscopic term in each subject by the use of an effective localized shimming procedure (14). Changes in image intensity reflect changes in the microscopic inhomogeneity. Furthermore, an increase in signal during stimulation, such as we have observed, implies that the field has become more homogeneous than in the prestimulation state. The exact mechanism giving magnetic resonance-visible changes remains to be elucidated; however blood flow and blood volume are known to increase during visual stimulation (5, 18, 19) and could be implicated. In the model of Ogawa *et al.* (6), in which the capillaries are approximated as cylinders with uniform susceptibility and infinite length, it can be shown that if capillary volume increases, total number of Hb molecules in the capillaries must decrease for the signal to increase. It is not sufficient for the fraction of Hb to decrease, rather the total number per tissue volume must decrease. Some insight may be gathered from the work of Grinvald and coworkers (18, 20), who used optical and infrared imaging of the exposed visual cortex in monkeys. They have shown during an 8-s stimulation period that the infrared absorption at 600 nm that is mainly due to Hb increases in a variable way, whereas the characteristic absorption of total hemoglobin (at the oxy- and deoxy-, isosbestic wavelength = 570 nm) increases. This latter time course is very similar to our magnetic resonance data, suggesting that the primary effect is blood-volume related and may reflect the associated increase in blood flow, reducing the Hb number. However, to determine the correlation requires an accurate deconvolution of their 600-nm absorption peak. We also studied a 2-s stimulation paradigm (protocol E), which can be compared to the data of Grinvald *et al.* (20), in which a monkey was stimulated visually for 1.5 s. Their optical data showed a short-lived increase in the total Hb, beginning shortly after the stimulus onset and peaking

after ≈ 2 s. This signal then returned to baseline with a subsequent overshoot (decrease in Hb below baseline) ≈ 3 s after the stimulus reaches a minimum at 6 s and lasts for 6 s. Basing the contrast mechanism in the magnetic resonance data purely on static Hb levels (i.e., excluding diffusion processes but including volume changes) suggests an initial decrease in signal followed by an increase. We observed only an increase in signal (Fig. 3), the time course of which corresponds to the undershoot in the infrared imaging data. Clearly simultaneous nuclear magnetic resonance and optical reflectance data under the same experimental conditions are needed to understand the dependence of the nuclear magnetic resonance signal upon the state of brain Hb.

Assuming that the signal changes are due to static susceptibility effects (i.e., there is no signal change from diffusion), then the expected signal in the baseline and stimulated cases can be described by simple exponential decays. S_0 is the signal in the absence of relaxation, and we define the echo time as TE and values of T_2^* for the two states. For compactness in the following expressions we have omitted the $*$. Let T_2 be the baseline value and $T_2^{\dagger}$ be the stimulated value, where

$$1/T_2^{\dagger} = 1/T_2 + 1/T_2^S,\qquad [1]$$

and $1/T_2^S$ is the change in relaxation rate during stimulation. The expression for the signal change ΔS is

$$\Delta S = S_0 \exp(-TE/T_2)[1 - \exp(-TE/T_2^S)],\qquad [2]$$

and the signal change relative to baseline is

$$\Delta S/S = 1 - \exp(-TE/T_2^S).\qquad [3]$$

It is noted that this is independent of the starting T_2, and measurements of $\Delta S/S$ can, therefore, be compared across studies. There are two parameters in Eq. 2—namely, TE and T_2. By simple differentiation, the value of TE that maximizes ΔS at a given T_2 is

$$TE_{\max} = T_2^S \ln[(T_2 + T_2^S)/T_2^S].\qquad [4]$$

In the limit that $T_2^S \gg T_2$, this reduces to $TE \approx T_2$. In collecting data, the important parameter is $\Delta S/N$, where N is noise. From Eq. 2 it is seen that this parameter depends only on TE and T_2 because T_2^S is a function of the stimulation. The magnitude of the signal change is, therefore, scaled by the exponential of TE/T_2, which depends on the macroscopic inhomogeneity of the shim field. Thus, we conclude that to maximize $\Delta S/N$, the sample should be optimally shimmed, and then an echo time (TE) should be selected to match the postshimming T_2^*. This result shows the importance of obtaining the best possible shim on each subject and will be especially true for studies of purely cognitive function where the positron emission tomography data have shown that blood flow effects are reduced severalfold relative to visual or motor-control stimulation paradigms (21).

Using Eq. 3 with our TE and mean value of $\Delta S/S$ gives T_2^S = 686 ms in our experiments. Substituting this value and our

measured value of T_2 into Eq. 4 gives $TE_{\max}$ = 67 ms, which is very close to our chosen TE. (The range of the calculated T_2^S given by ± 1 SD is 525 ms $-$ 980 ms.)

In conclusion, high-speed gradient-echo magnetic resonance imaging is highly sensitive to changes in the local magnetic fields within the human brain that occur during increased activity associated with visual stimulation. Although the mechanisms involved are not fully understood, the high sensitivity of the technique will allow it to be used to form high-resolution maps of functional changes in humans on an individual basis without the need for inter-subject averaging.

1. Rosen, B. R., Belliveau, J. W., Vevea, J. M. & Brady, T. J. (1990) *Magn. Reson. Med.* 14, 249–265.
2. Mansfield, P. (1977) *J. Phys. C* 10, L55–L58.
3. Haase, A., Frahm, J., Matthaei, D., Hanicke, W. & Merboldt, K. D. (1986) *J. Magn. Reson.* 67, 258–266.
4. Meier, P. & Zierler, K. L. (1954) *J. Appl. Physiol.* 6, 731–744.
5. Belliveau, J. W., Kennedy, D. N., McKinstry, R. C., Buchbinder, B. R., Weisskoff, R. M., Cohen, M. S., Vevea, J. M., Brady, T. J. & Rosen, B. R. (1991) *Science* 254, 716–719.
6. Ogawa, S., Lee, T. M., Nayak, A. S. & Glynn, P. (1990) *Magn. Reson. Med.* 14, 68–78.
7. Ogawa, S., Lee, T. M., Kay, A. R. & Tank, D. W. (1990) *Proc. Natl. Acad. Sci. USA* 87, 9868–9872.
8. Turner, R., Le Bihan, D., Moonen, C. T. W., Despres, D. & Frank, J. (1991) *Magn. Reson. Med.* 22, 159–166.
9. Ogawa, S., Tank, D. W., Menon, R., Ellermann, J., Kim, S.-G., Merkle, H. & Ugurbil, K. (1992) *Proc. Natl. Acad. Sci. USA* 89, 5951–5955.
10. Kwong, K. K., Belliveau, J. W., Chesler, D. A., Goldberg, I. A., Weisskoff, R. M., Poncelet, B. P., Kennedy, D. N., Hoppel, B. E., Cohen, M. S., Turner, R., Cheng, H.-M., Brady, T. J. & Rosen, B. R. (1992) *Proc. Natl. Acad. Sci. USA* 89, 5675–5679.
11. Bandettini, P. A., Wong, E. C., Hinks, R. S., Tikofsky, R. S. & Hyde, J. S. (1992) *Magn. Reson. Med.* 25, 390–397.
12. Blamire, A. M. & Shulman, R. G. (1992) *Soc. Magn. Reson. Med. Abstr.* 11, 4516.
13. Mansfield, P. & Chapman, B. (1986) *J. Magn. Reson.* 66, 573–576.
14. Gruetter, R. & Boesch, Ch. (1992) *J. Magn. Reson.* 96, 323–334.
15. Ljunggren, S. (1983) *J. Magn. Reson.* 54, 338–343.
16. Fox, P. T. & Raichle, M. E. (1985) *Ann. Neurol.* 17, 303–305.
17. Kim, W. S. & Cho, Z. H. (1992) *Magn. Reson. Med.* 24, 162–188.
18. Frostig, R. D., Lieke, E. E., Ts'o, D. Y. & Grinvald, A. (1990) *Proc. Natl. Acad. Sci. USA* 87, 6082–6086.
19. Fox, P. T., Raichle, M. E., Mintun, M. A. & Dence, C. (1988) *Science* 241, 462–464.
20. Grinvald, A., Lieke, E., Frostig, R. D., Gilbert, C. D. & Wiesel, T. N. (1986) *Nature (London)* 424, 361–364.
21. Petersen, S. E., Fox, P. T., Posner, M. I., Mintun, M. & Raichle, M. E. (1988) *Nature (London)* 331, 585–589.